Microstructure and mechanical properties of an Fe–Mn–Al–C lightweight steel after dynamic plastic deformation processing and subsequent aging

Zongyuan Li[a], Ying Chun Wang[a,b,*] , Xingwang Cheng[a,b], Chong Gao[a], Zhuang Li[a], Terence G. Langdon[c]
[a]*School of Materials Science and Engineering, Beijing Institute of Technology, Beijing 100081, China*
[b]*National Key Laboratory of Science and Technology on Materials under Shock and Impact, Beijing 100081, China*
[c]*Materials Research Group, Department of Mechanical Engineering, University of Southampton, Southampton SO17 1BJ, UK*

Abstract

An austenitic low-density steel was processed by dynamic plastic deformation (DPD) over the strain range from 0.25 to 0.75 followed by aging at 450°C and then it was subjected to compressive testing at strain rates of $1.0 \times 10^{-3} - 2.0 \times 10^{3}$ s^{-1}. The results show that fine grain structures with high density dislocations are achieved after DPD processing. After aging, the grain size increased slightly together and there was an additional marginal decrease in the dislocation density. κ-carbides only appeared in the samples after DPD processing at the strain of 0.75 and after subsequent aging. Submicron-sized (Nb, Mo)C particles existed in the matrix before DPD and there was no change in size and distribution during DPD processing and post-DPD aging. The yield strengths of the steels after DPD at different strain rates increased significantly by ~120-190% compared with the as-received sample, where this is mainly due to a combination of dislocation strengthening and grain boundary strengthening. For the steel processed by DPD at strain of 0.75, there was an additional precipitation strengthening of κ-carbides besides the dislocation strengthening and grain boundary strengthening, and this produced an increase of over ~900 MPa in yield strength by comparison with the as-received steel. After aging, the yield strength decreased slightly due to a reduction in the dislocation density and a slight coarsening of the grains, except for samples after DPD at a strain of 0.75 which showed a slight increase in strength due to further κ precipitation. The strain rate strengthening effect and strain hardening ability were also analyzed.

Keywords: Lightweight steels; Dynamic plastic deformation; Aging; Mechanical properties; Strengthening mechanisms

*Corresponding author: Ying Chun Wang, e-mail: wangyc@bit.edu.cn

1. Introduction

Dynamic plastic deformation (DPD) has proven to be a promising method for achieving ultrafine grained (UFG) structures by severe deformation at high strain rates of $10^2 \sim 10^3$ s^{-1} [1-4]. Several DPD processing methods have been developed such as high-speed hammer or split Hopkinson pressure bar (SHPB) impacting[5],[6], dynamic high-pressure torsion (DHPT) [7], and dynamic channel angular pressing (DCAP) [8]. Of these procedures, SHPB impacting is a particularly effective method for producing UFG materials by impacting samples at high strain rates of $\sim 10^3$ s^{-1} for several presses [5].

There are several reports available documenting the microstructure evolution and mechanical properties improvement of different materials after DPD processing, such as pure Cu [9-13], Ti [14-16], aluminum alloys [1, 3, 17-24] and steels [2, 4, 25-30]. Some of these studies showed that steels were significantly strengthened by grain refinement after DPD processing [4, 26]. For example, the average grain size of a commercial 20MnSiV steel decreased from ~30 μm to ~1.75 μm through DPD and this produced an increase in the yield strength by ~28% compared with the as-received sample [28]. A recent report demonstrated that DPD processing at a strain of 2.3 led to an increase in the dislocation density and the formation of a finer dislocation cell structure in a 9Cr-1Mo steel and this gave an improvement in the ultimate tensile strength from 675 MPa to 1247 MPa [26]. Another study found that after DPD processing at a strain of 1.7 and subsequent annealing the microstructure of a plain low-carbon steel was primarily of lamellar structures having an average thickness of ~84 nm and this was combined with the existence of well-dispersed fine carbide precipitates within the matrix and a high density of dislocations which also led to an obvious enhancement in the tensile strength [27]. Thus, it is readily concluded that DPD processing for steels may effectively refine the grains, increase the dislocation density, promote the occurrence of precipitation and thereby enhance the mechanical properties.

The Fe-Mn-Al-C austenitic low-density steels have major application prospects in the automobile industry due to their high strength, good plasticity, excellent resistance to corrosion

and low density[31-34]. Nevertheless, there is a significant interest in further improving the mechanical properties of austenitic low-density steels in order to meet the ever more stringent requirements for vehicular safety combined with lower fuel consumption[35-38]. Deformation followed by aging is an effective process for strengthening low-density steels[33, 39-41]. For example, a 20% rolling processing improved the yield strength of an Fe-23.38Mn-6.86Al-1.43C-0.038Nb-0.29Mo steel by ~500 MPa due to the dislocation strengthening[39]. In a recent report, the promotion of κ-carbide precipitation after 20% cold rolling and aging at 550°C in Fe-20Mn-9Al-1.2C-1V led to a further enhancement of ~100 MPa in yield strength compared with the strength before aging[41]. It can be summarized that deformation and subsequent aging increases the strength of low-density steels by increasing the dislocations density and promoting κ precipitation. By comparison with conventional hot or cold deformation, DPD processing at a much higher strain rate can additionally refine the grains. The mechanical properties of the Fe-Mn-Al-C austenitic low-density steels may be further significantly enhanced through a combination of multiple strengthening mechanisms after DPD. However, it is surprising to note that no reports are available to date on the strengthening of low-density steels by DPD. In addition, the Fe-Mn-Al-C austenitic low-density steels are mainly used as vehicle shells and these shells may be subjected to dynamic loading during service as, for example, in driving collisions [31, 42]. Accordingly, it is reasonable to conclude that an understanding of the behavior of austenitic low-density steels under different strain rates will be important for developing future engineering applications.

Based on the obvious need for experimental data in this area, the present investigation was initiated to examine the effect of DPD processing and subsequent aging on the microstructural evolution and the compressive behavior of an Fe-Mn-Al-C lightweight steel under strain rates within the range from 1.0×10^{-3} to 2.0×10^{3} s^{-1}.

2. Experimental material and procedures

This study used a steel having a chemical composition of Fe-26Mn-8Al-0.8C-0.1Nb-0.3Mo (wt.%) which was cast after vacuum melting in an Ar atmosphere. The steel ingot was

forged at 900-1100°C into a round bar of ~12 mm diameter and then cooled in air. It was then cut into cylinders with diameters of 11 mm and heights of 18 mm and solution-treated at 1000°C for 1 h followed by water quenching before DPD. Subsequently, the cylinders were processed by DPD on a SHPB facility at room temperature (RT, ~298 K) with a strain rate of ~10^3 s^{-1} under uniaxial compression. The steel was processed to 2, 4 and 8 times of impacts to reach strains of ~0.25, ~0.5 and ~0.75 where the strain was defined as ln (L_0 / L_f), where L_0 and L_f are the cylinder heights before and after the DPD processing, respectively. Following DPD, samples were aged at 450°C for 2 h and then cooled in air. For convenience, the steels processed by DPD for strains of 0.25, 0.50 and 0.75 are henceforth denoted as DPD-0.25, DPD-0.50 and DPD-0.75 and the corresponding post-DPD aged steels are designated DPD-0.25-450, DPD-0.50-450 and DPD-0.75-450, respectively.

Compressive specimens with diameters of 5 mm and heights of 4 mm were cut from both the DPD-processed and the aged samples. Compression testing was carried out at RT using an Instron testing machine operating with a strain rate of 1.0 × 10^{-3} s^{-1}, a Gleeble 3500 thermal simulator with a strain rate of 1.0 × 10^0 s^{-1} and a split Hopkinson pressure bar with a strain rate of 2.0 × 10^3 s^{-1}. For verifying repeatability, three compression specimens were tested for each condition. The microstructures were analyzed by X-ray diffraction (XRD, Bruker D8 Advance), scanning electron microscopy (SEM, Hitachi S4800), electron backscatter diffraction (EBSD, FEI Quanta 650F) and transmission electron microscopy (TEM, Tecnai F20) on surfaces parallel to the compression direction. The XRD analysis was performed using Cu Kα radiation (λ=0.1542 nm) with a scanning speed of 1°/min covering 2θ from 20° to 90°. The EBSD specimens were mechanically polished and electro-polished at room temperature in a 93% CH_3COOH + 7% $HClO_4$ solution with an operating current density of 450 mA/cm^2. The step size during EBSD was set at 0.2 μm and the results were analyzed with Channel 5 software. The average grain size was calculated by the equivalent grain size method from EBSD maps based on grain boundaries with threshold misorientation angles of >15°. The samples were prepared for TEM by electro-polishing in an electrolyte of 90% methanol and

10% perchloric acid (vol%) using a voltage of 20 V at −30°C.

The volume fraction of the precipitates was estimated by the following equation[43]:

$$f = V * N/(S * 2d) \quad (1)$$

where *f* is the volume fraction of the precipitates in the microstructure, *V* is the average volume of the precipitates, *N* is the number of precipitates within the statistical area, *S* is the area size of the statistical area and *d* is the average size of the precipitates.

The dislocation density ρ was calculated from the XRD results through Equation [44]:

$$\Delta K = \frac{0.9}{D} + \left(\pi A^2 \frac{b^2}{2}\right)^{\frac{1}{2}} \rho^{\frac{1}{2}} \left(K\bar{C}^{\frac{1}{2}}\right) \quad (2)$$

where ΔK is the half-peak width of the XRD pattern, D is the average grain size of the sample, A is an infinite compensational constant depending on the effective outer cut-off radius of the dislocation where $A = 2$ in this investigation [45], b is the Burgers vector, K is the peak position and $\bar{C}$ is the average contrast factor of the dislocation on a specific crystal plane. The specific calculation methods for the parameters of ΔK, K and $\bar{C}$ were reported elsewhere [44].

3 Experimental results

3.1 Microstructures characterization

Fig.1 shows XRD patterns of the steels which reveals that the microstructures of all samples remain unchanged as austenite. Figs 2 and 3 show the EBSD orientation color-coded maps of the as-received and the DPD-processed and post-DPD aged samples, respectively, and Fig.4 displays the corresponding grain size distributions. Inspection of Fig.2 shows the as-received steel has equiaxed austenitic grains with an average grain size of ~31.6 μm and with random orientations. After DPD processing, the austenitic grains shown in Fig. 3(a)-(c) are refined by the DPD and the grain sizes decrease with increasing strain but nevertheless they retain an overall equiaxed morphology with a tendency towards a <111> orientation. Fig.3(b) and (c) show that many fine grains are observed together with the presence of a few coarse grains after DPD processing at strains over 0.5. Fig.4 (a)-(c) shows grain size distributions of

the steel after DPD. The measurements show that the average grains sizes are ~9.1 μm, ~5.3 μm and ~3.1 μm for the DPD-0.25, DPD-0.50 and DPD-0.75 samples, respectively. Inspection of Fig.2 and Fig.3 also shows there are twins within a few grains and the number of twins remains essentially unchanged before and after DPD processing, which means that these twins in the austenitic grains are from original microstructure and the TWIP effect does not occur. This is because the calculated stacking fault energy (SFE) of the steel is ~71 mJ/m^2 according to the modified Olson-Cohen thermo-dynamical model [46, 47] and this is higher than ~20-40 mJ/m^2 required for the formation of deformation twinning [39]. Post-DPD aging leads to an increase in the grain sizes, especially for the coarser grains shown in Fig. 3(d)-(f) and Fig.4(d)-(f) by comparison with the microstructures before aging. The mean grain sizes of the DPD-0.25-450, DPD-0.50-450 and DPD-0.75-450 samples were recorded as ~10.6 μm, ~6.9 μm and ~7.3 μm, respectively. Additionally, further observation of Figs 3 and 4 reveals that after aging processing a few grains with large sizes over ~40 μm in the DPD-0.50-450 and DPD-0.75-450 samples appear thereby showing an abnormal grain growth.

Fig.5 presents bright field TEM images of the DPD-processed and post-DPD aged samples showing the dislocation configuration. Inspection of Fig. 5(a), (b) and (c) shows that the dislocations are entangled and their density increases as the strain increases from 0.25 to 0.75. Based on XRD, the dislocation densities were quantitatively calculated as 1.0×10^{15}, 1.37×10^{15} and $1.60 \times 10^{15}/m^2$ for the DPD-0.25, DPD-0.50 and DPD-0.75 samples, respectively. An examination of Fig.5 (d)-(f) shows that the dislocation configurations remain essentially unchanged but the dislocation densities are reduced after aging to 0.90×10^{15}, 1.30×10^{15} and $1.55 \times 10^{15}/m^2$ in the DPD-0.25-450, DPD-0.50-450 and DPD-0.75-450 steels, respectively.

Fig. 6 depicts SEM images of the as-received, DPD-0.25, DPD-0.75 and DPD-0.75-450 samples showing there are granular precipitates with average diameters of ~300 nm distributed within the austenitic matrix. These precipitates were identified as (Nb, Mo)C carbides in an earlier study [48]. Further observation shows that the sizes and distributions of the particles in

both the DPD-processed and the post-DPD aged steels remain unchanged due to their high thermodynamic stability [48]. There is no evidence for the presence of κ carbides in the DPD-0.25 and DPD-0.50 samples but they are present in the DPD-0.75 and DPD-0.75-450 samples as demonstrated by the dark field TEM images in Fig. 7[36, 49]. Figs 7(a) and (b) show that these nano-scale κ-carbides are spherical and uniformly distributed within the matrix. The statistical data shows that the mean size and volume fraction of κ increased from ~0.3 nm and 1.0% after DPD processing to ~2.0 nm and 6.6% after subsequent aging, respectively.

3.2 Compressive properties

Fig. 8 shows the true stress-true strain curves of the as-received, DPD-processed and the post-DPD aged samples for strain rates of (a) 1.0×10^{-3}, (b) 1.0×10^{0} and (c) 2.0×10^{3} s^{-1} and Fig.9 shows the effects of DPD processing and post-DPD aging on the relevant yield strengths. It is readily apparent in Fig.9(a)-(c) that the yield strengths of both the DPD-processed and the post-DPD aged steels are significantly improved by comparison with the as-received steel and the yield strengths are further enhanced by DPD straining. Specifically, when the DPD strain increases from 0.25 to 0.75 the yield strengths increase by ~120-190% (~568-910 MPa) at 1.0×10^{-3} s^{-1}, ~90-170% (~536-1002 MPa) at 1.0×10^{0} s^{-1} and ~110-155% (~719-1187 MPa) at 2.0×10^{3} s^{-1}, respectively, by comparison with the as-received steel. For the DPD-0.75 steels, the increment in strength is more than 900 MPa under these experimental conditions. This demonstrates that DPD processing introduces a very significant strengthening in the Fe-Mn-Al-C lightweight steel. A post-DPD aging leads to a slight reduction in the yield strength for the DPD-0.25 and DPD-0.50 steels but a minor increase for the DPD-0.75 steel.

Fig. 8(a) and (b) show the flow stresses of the as-received sample at strain rates of 1.0×10^{-3} and 1.0×10^{0} s^{-1} increase continuously with strain and exhibit a strain hardening ability due to the lower dislocation density and the absence of precipitation of the κ-carbides. For the DPD-0.25 steel the strain hardening ability is lower than for the as-received condition but remains positive due to the increase in the dislocation density. As the strain further increases to 0.75, more dislocations multiply and this is coupled with κ precipitation which decreases

the strain hardening ability giving a balance between thermal softening and strain hardening. Fig. 8(c) demonstrates that the as-received sample maintains a good strain hardening ability during dynamic testing at a strain rate of 2.0×10^3 s^{-1}. However, the strain hardening ability decreases initially and then increases for the DPD-processed and post-DPD aged samples. The first decrease in the strain hardening ability is a consequence of the adiabatic temperature rise which assists the thermal softening and by the cutting of more κ-carbides by dislocations at the higher strain rates [48]. The reappearance of a hardening effect in the curves is attributed to the further DPD processing for the compressive samples during the dynamic testing.

Further inspection of Fig.8(a), (b) and (c) shows the yield strength increases with increasing strain rate, thereby confirming a strain rate strengthening effect. The yield strength increases by ~100-200 MPa for the as-received and DPD-processed steels when the strain rate increases from 1.0×10^{-3} to 1.0×10^0 s^{-1} and from 1.0×10^0 to 2.0×10^3 s^{-1}. The post-DPD aged steels also exhibit an increase of ~100-200 MPa in strength when the strain rate increases from 1.0×10^{-3} to 1.0×10^0 s^{-1}. Nevertheless, an increase in strain rate from 1.0×10^0 to 2.0×10^3 s^{-1} only increases the yield strength by ~30-40 MPa for both the DPD-0.25-450 and DPD-0.50-450 samples while there is an increase by 165 MPa for the DPD-0.75-450 sample.

4. Discussion

4.1 Microstructural evolution

Fig. 3 shows that the grains are equiaxed and the numbers of grains increase after DPD processing, therefore it is concluded that dynamic recrystallization occurred. The increasing density of dislocations provides more stored energy and promotes the occurrence of dynamic recrystallization with increasing DPD strain and this leads to a decrease in grain size. Notably, the grain sizes are inhomogeneous after DPD processing to strains over 0.5 and post-DPD aging and this is due to the presence of the non-shearable (Nb, Mo)C particles before DPD processing. Dislocations pile up around these particles and the stored energy accumulating in local areas leads to a growth in the recrystallized grains [39].

No κ-carbides were detected in the DPD-0.25, DPD-0.50, DPD-0.25-450 and DPD-0.50-

450 samples but they are present in the DPD-0.75 and DPD-0.75-450 samples as shown in Fig.7. Generally, for Fe-Mn-Al-C lightweight steels with a carbon content of 0.8 the kinetics of the κ precipitation is weak and the available evidence suggests that κ may only precipitate during aging above 600℃ for 2 h or at 500 ℃ for more than 6 hours [49-53], and the volume fraction of κ is only about 2%[41, 54]. However, the volume content of κ in the DPD-0.75-450 samples reached ~6%, indicating DPD processing promotes the κ precipitation. Apparently, there is an insufficient driving force for κ precipitation in the DPD-0.25 and DPD-0.50 samples during DPD even after aging at 450℃ for 2 hours. For DPD processing at the higher strain of 0.75, where the sample was pressed for 8 times at ~10^3 s^{-1}, due to the high resistance of deformation there is an increase in the stored energy and this leads to the occurrence of dynamic precipitation of κ in the DPD-0.75 sample and further precipitation after aging. On the other hand, since κ are formed by spinodal decomposition, dislocations can promote κ precipitation by accelerating atomic diffusion. Samples at a strain of 0.75 contain the highest dislocation density resulting in κ precipitation [39].

4.2 Strengthening mechanism of the DPD steel

After subjecting the steel to DPD processing and a subsequent aging treatment, the major contributions to the strength come from dislocation strengthening, σ_d, κ precipitation strengthening, σ_p, and grain boundary strengthening, σ_g. In addition to these three strengthening mechanisms, the precipitation strengthening from Nb/Mo carbides and solid solution strengthening are also involved in the experimental steels. Since the composition of the steel remains unchanged under the present experiment condition, the contribution of solid solution strengthening may be regarded as the same for all samples. The precipitation enhancement caused by the Nb/Mo carbides may also be regarded as a constant since there is no change in these carbides before and after DPD processing and in post-DPD aging as shown in Fig. 6. To a first approximation, the contribution of both solid solution strengthening and precipitation strengthening from the (Nb, Mo)C carbides is equal to 345 MPa where this corresponds to σ_0. This was calculated from the strength of the as-received sample subtracted

from the value for the grain boundary strengthening for the as-received sample as defined in the form $\sigma_0 = \sigma_{s\text{-}as\text{-}received} - \sigma_{g\text{-}as\text{-}received}$. The significance of the other three strengthening mechanisms is now examined in the following sections.

4.2.1 Dislocation strengthening

The contribution of the dislocations to the yield strength is given by [41]

$$\sigma_d = \alpha M G b \rho^{\frac{1}{2}} \tag{3}$$

where α is a constant related to the material properties and has a value of 0.24, M is the orientation factor which is equal to 3.06 for FCC materials, G is the shear modulus of austenite which is taken as 70.7 GPa and b is the modulus of the Burgers vector of austenite having a value of 0.26 nm [41, 43, 55]. According to Eq. (3), the calculated values of σ_d are in the range of ~427-540 MPa after DPD processing for a strain of 0.25-0.75. After subsequent aging, the significance of dislocation strengthening decreases slightly but remains over 400 MPa。

4.2.2 Precipitation strengthening by κ carbides

The κ carbides were found only in the DPD-0.75 and DPD-0.75-450 samples shown in Fig. 7. Thus, the DPD-0.75 and DPD-0.75-450 samples have an additional precipitation strengthening from the presence of these carbides.

Precipitation strengthening originates from the interaction between the dislocations and the precipitates. It is well known that the κ precipitates can be cut by mobile dislocations during loading. This type of strengthening may be divided into order strengthening (σ_{po}), coherency strengthening (σ_{pc}) and modulus mismatch strengthening (σ_{pm}) where these various terms are expressed by the following equations [41, 43, 56]:

$$\sigma_{po} = 0.81 M \frac{\gamma_{APB}}{2b}\left(\frac{3\pi f}{8}\right)^{\frac{1}{2}} \tag{4}$$

$$\sigma_{pc} = M\chi(G\varepsilon)^{\frac{3}{2}}\left(\frac{2rf}{Gb}\right)^{\frac{1}{2}} \tag{5}$$

and

$$\sigma_{pm} = 0.0055M(\Delta G)^{\frac{3}{2}}\left(\frac{2f}{Gb^2}\right)^{\frac{1}{2}} b\left(\frac{r}{b}\right)^{\frac{3}{2}m-1} \quad (6)$$

where γ_{APB} is the average antiphase boundary energy which is 0.2 J/m^2, r is the mean nano-precipitate radius, f is the volume fraction of the precipitates, ε is the constrained lattice parameter mismatch which is 0.574%, χ and m are constants having values of 2 and 0.85, respectively, and ΔG is the shear modulus mismatch which is 23.7 GPa [41, 43, 55].

The improvement value of the yield strength induced by the shearing mechanism takes the larger of either σ_{po} or $\sigma_{pc}+\sigma_{pm}$. By calculation it can be shown that σ_{po} is dominant for both samples. Therefore, the calculated strength increments from κ precipitation for the DPD-0.75 and DPD-0.75-450 steels are ~101 MPa and ~266 MPa, respectively. Furthermore, additional precipitation during post-DPD aging leads to an increase in strength by 165 MPa.

4.2.3 Grain boundary strengthening

The DPD processing produces a reduction in the grain size and therefore it strengthens the material. The contribution of the refined grain size to the strength is described directly by the Hall-Petch relationship which gives [41, 43, 55]:

$$\sigma_g = kd^{-\frac{1}{2}} \quad (7)$$

where k is ~683 MPa·μm$^{1/2}$ for steels [41, 43, 55]. Through Eq.(7), it is calculated that the increases in strength from grain boundary strengthening for the DPD processing at strains from 0.25 to 0.75 are ~226-389 MPa by comparison with the as-received material. After subsequent aging, the increase decreases by ~16-136 MPa compared to the DPD-processed samples.

4.2.4 Overall effect of strengthening

The calculated results for the dislocation strengthening, precipitation strengthening and grain boundary strengthening are shown in Fig. 10 and Table 1. These results demonstrate that the yield strengths of the DPD-processed steels are significantly enhanced compared with the as-received steel and they are even further increased with straining. This is due to a combination of grain refinement strengthening and dislocation strengthening for the DPD-

0.25, DPD-0.50, DPD-0.25-450 and DPD-0.50-450 steels while there is also an additional precipitation strengthening from κ precipitation for the DPD-0.75 and DPD-0.75-450 steels. Post-DPD aging of the DPD-0.25 and DPD-0.50 samples leads to a reduction in strength by ~10-40 MPa and ~10-20 MPa, respectively, due to grain coarsening and dislocation recovery by comparison with the DPD-processed steels. Nevertheless, the strength of DPD-0.75-450 steel is higher than the DPD-0.75 steel due to the additional precipitation strengthening from the κ carbides of ~165 MPa which compensates for the strength loss caused by the grain coarsening and the dislocation density decrease during the post-DPD aging.

4.3 Effect of strain rate on compression behavior

A comparison of the yield strengths from tests at strain rates from 1.0×10^{-3} to 2.0×10^{3} s^{-1} in Fig. 8 shows that the steels exhibit a strain rate strengthening effect. The strain rate sensitivity (SRS) can be expressed as [48, 57]:

$$ln\dot{\varepsilon} = \left(\sigma - \sigma_{\mu}\right) \cdot \frac{V^*}{Mk_BT} + ln\dot{\varepsilon}_0 - \frac{\Delta G_0}{k_BT} \tag{8}$$

where $\dot{\varepsilon}$ is the strain rate, σ is the total yield stress, σ_{μ} is the athermal component of σ, V^* is the activation volume of the moving dislocations, M is the average Taylor factor, k_B is the Boltzmann constant, T is the absolute temperature, $\dot{\varepsilon}_0$ is the pre-exponential factor, and ΔG_0 is Helmholtz free energy (activation energy).

Eq. (8) can be simplified as [48]:

$$ln\dot{\varepsilon} = K\sigma + B \tag{9}$$

where $K = \frac{V^*}{Mk_BT}$, which reflects the SRS and a smaller K value represents a higher strain rate sensitivity of the yield strength and $B = ln\dot{\varepsilon}_0 - \frac{M\Delta G_0 + V^*\sigma_{\mu}}{Mk_BT}$ which is regarded as a constant.

The $ln\dot{\varepsilon}$-σ relationship was linear fitted as shown in Fig. 11 and it displays a yield stress σ that basically has a linear relationship with $ln\dot{\varepsilon}$. Specifically, the as-received steel presents the largest K value implying a minimum SRS. With increasing DPD strain, K decreases which indicates that the SRS increases. A post-DPD aging leads to a decrease in SRS for the DPD-

0.25 and DPD-0.50 steels but an increase for the DPD-0.75 steel.

In Eq. (9), $K = \frac{V^*}{Mk_BT}$. Thus, K is affected by the activation volume of the moving dislocations V^*, which can be defined as [48]:

$$V^* = b \cdot \xi \cdot l^* \tag{10}$$

where b is the Burgers vector of the dislocations, ξ is the distance swept out by the mobile dislocation during one activation event, and l^* is the length which scales with the average contact distance between two obstacles[48]. Since the Burgers vector b is a constant, the value of K depends on the product of ξ and l^*, which increases with the dislocation density decreasing and with grain coarsening.

The as-received steel has the lower dislocation density and the larger grain size which increases the $\xi \cdot l^*$ resulting in the lowest SRS according to Eq. (10) compared to the DPD-processed steels. For the DPD processed steels, with strain increasing the SRS tends to increase because both the dislocation density increases and the grain refinement makes the value of $\xi \cdot l^*$ decrease in Eq. (10), which means the SRS increases. In addition, Fig. 11 shows that the SRS of DPD-0.25-450 and DPD-0.50-450 decrease by comparison with DPD-0.25 and DPD-0.50, respectively, which is mainly attributed to the decrease of dislocations and the grain coarsening. However, the SRS of the DPD-0.75-450 sample is more sensitive than DPD-0.75 and this is because of the presence of more κ-carbides precipitated during the post-DPD aging where this leads to a significant reduction in l^* in Eq. (10) which offsets the effect of dislocation recovery and grain coarsening and thereby leads to an increment in SRS [24, 48].

Overall, these results show that the various SRS of the Fe-Mn-Al-C lightweight steel depend primarily on the difference in dislocation density, grain size and the appearance of precipitates. In addition, the dislocation density increase, grain refinement and κ precipitation after DPD processing lead to a significant strain rate strengthening effect for the steel.

5. Summary and conclusions

Experiments were conducted to investigate the microstructural evolution and the mechanical behavior at strain rates from 1.0×10^{-3} to 2.0×10^{3} s^{-1} for the Fe-26Mn-8Al-0.8C-0.1Nb-0.3Mo lightweight steel after DPD processing for strains in the range of 0.25-0.75 and post-DPD annealing at 450°C. The main conclusions are as follows.

1. DPD processing produces a fine-grained structure with an average grain size of ~3 μm and nano-sized κ-carbides of ~0.30 nm distributed evenly in the matrix together with a high density of dislocations after DPD for a strain of 0.75. Post-DPD aging slightly increases the grain size and decreases the dislocation density. Submicron-sized (Nb, Mo)C particles exist in the matrix before DPD and there is no change in size and distribution during DPD processing and post-DPD aging.

2. The yield strength at different strain rates of the steels after DPD is significantly increased by ~120-190 % compared with the as-received sample, and this is mainly due to a combination of dislocation strengthening and grain boundary strengthening. For the steel subjected to DPD processing at a strain of 0.75, there is an additional precipitation strengthening of κ-carbides which adds to the dislocation strengthening and grain boundary strengthening and leads to an increase in the yield strength of over 900 MPa compared with the as-received steel. After aging, the yield strength decreased slightly due to a reduction in the dislocation density and a slight coarsening of the grains, except for samples after DPD at a strain of 0.75 which exhibited a slight increase in strength due to further κ precipitation.

3. DPD processing and increasing the DPD strain leads to an increase in the strain rate sensitivity due to the combined effect of dislocation multiplication and grain refinement. Post-DPD aging leads to a decrease in the SRS for the DPD-0.25 and DPD-0.50 samples because of dislocation recovery and grain coarsening but there is an increase for the DPD-0.75 sample due to a further precipitation of κ-carbides which reduces the average contact distance between two obstacles and this further counteracts the effect of the dislocation density decrease and grain coarsening.

Declaration of competing interest

The authors declare that they have no known competing financial interests or personal relationships that could have appeared to influence the work reported in this paper.

CRediT authorship contribution statement

Zongyuan Li: Conceptualization, Validation, Formal analysis, Investigation, Writing-original draft, Writing-review & editing. Yingchun Wang: Conceptualization, Formal analysis, Writing-review & editing, Supervision. Xingwang Cheng: Project administration, Funding acquisition, Supervision. Chong Gao: Investigation. Zhuang Li: Investigation. Terence G Langdon: Writing-review & editing, Supervision.

Acknowledgements

The work was supported by the funding of National Science and Technology Major Project (J2019-VI-0019-0134), the National Natural Science Foundation of China under Grant No. 51671030 and the European Research Council under Grant Agreement No. 267464-SPDMETALS (TGL).

References

[1] S.B. Jin, N.R. Tao, K. Marthinsen, Y.J. Li, Deformation of an Al-7Mg alloy with extensive structural micro-segregations during dynamic plastic deformation, Mater. Sci. Eng. A 628 (2015) 160-167.

[2] B. Wang, B. Yao, Z. Han, Annealing effect on wear resistance of nanostructured 316L stainless steel subjected to dynamic plastic deformation, J. Mater. Sci. Technol. 28 (2012) 871-877.

[3] F. Huang, N.R. Tao, K. Lu, Effects of strain rate and deformation temperature on microstructures and hardness in plastically deformed pure aluminum, J. Mater. Sci. Technol. 27 (2011) 1-7.

[4] Z.B. Zhang, O.V. Mishin, N.R. Tao, W. Pantleon, Effect of dynamic plastic deformation on microstructure and annealing behaviour of modified 9Cr-1Mo steel, Mater. Sci. Technol. 31 (2014) 715-721.

[5] Y. Yang, Y.D. Chen, F. Ma, H.B. Hu, Q.M. Zhang, T.G.Tang, X.W. Zhang, Microstructure evolution of 1050 commercial purity aluminum processed by high-strain-rate deformation. J. Mater. Eng. Perform. 24 (2015) 4307-4312.

[6] L. Farbaniec, A.A Latif, J. Gubicza, G. Dirras, High purity ultrafine-grained nickel processed by dynamic plastic deformation: microstructure and mechanical properties, Adv. Eng. Mater. 14 (2012):1027-1033.

[7] P. Verleysen, H. Lanjewar, Dynamic high pressure torsion: a novel method for high strain rate severe plastic deformation, J. Mater. Process. Tech. 276 (2020) 116393

[8] J.H. Han, J.Y. Suh, K.K. Jee, J.C. Lee, Evaluation of formability and planar anisotropy based on textures in aluminum alloys processed by a shear deforming process. Mater. Sci. Eng. 477 (2008) 107-120.

[9] Y.S. Li, Y. Zhang, N.R. Tao, K. Lu, Effect of thermal annealing on mechanical properties of a nanostructured copper prepared by means of dynamic plastic deformation, Scr. Mater. 59 (2008) 475-478.

[10] W.S. Zhao, N.R. TAO, J.Y. Guo, Q.H. Lu, K. Lu, High density nano-scale twins in Cu induced by dynamic plastic deformation. Scr. Mater. 53 (2005) 745-749.

[11] Y.S. Li, N.R. Tao, K. Lu, Microstructural evolution and nanostructure formation in copper during dynamic plastic deformation at cryogenic temperatures, Acta Mater. 56 (2008) 230-241.

[12] B. Yao, Z. Han, Y.S. Li, N.R. Tao, K. Lu, Dry sliding tribological properties of nanostructured copper subjected to dynamic plastic deformation, Wear 271 (2011) 1609-1616.

[13] H.L. Wang, Z.B. Wang, K. Lu, Interfacial diffusion in a nanostructured Cu produced by means of dynamic plastic deformation, Acta Mater. 59 (2011) 1818-1828.

[14] C.L. Wang, D.P. Yu, Z.Q. Niu, W.L. Zhou, G.Q. Chen, Z.Q. Li, X.S. Fu, The role of pyramidal < c + a > dislocations in the grain refinement mechanism in Ti-6Al-4V alloy processed by severe plastic deformation, Acta Mater. 200 (2020) 101-115.

[15] F. Xu, X.Y. Zhang, H.T. Ni, Y.M. Cheng, Y.T. Zhu, Q. Liu, Effect of twinning on microstructure and texture evolutions of pure Ti during dynamic plastic deformation. Mater. Sci. Eng. A 564 (2013) 22-33

[16] J.L. Sun, P.W. Trimby, X. Si, X.Z. Liao, N.R. Tao, J.T. Wang, Nano twins in ultrafine-grained Ti processed by dynamic plastic deformation. Scr. Mater. 68 (2013) 475-478.

[17] F. Huang, N.R. Tao, K. Lu, Effects of impurity on microstructure and hardness in pure al subjected to dynamic plastic deformation at cryogenic temperature, J. Mater. Sci. Technol. 27 (2011) 628-632.

[18] K.O. Pedersen, T. Børvik, O.S. Hopperstad, Fracture mechanisms of aluminium alloy AA7075-T651 under various loading conditions, Mater. Des. 32 (2011) 97-107.

[19] E. El-Magd, M. Brodmann, Influence of precipitates on ductile fracture of aluminium alloy AA7075 at high strain rates, Mater. Sci. Eng. A 307 (2001) 143-150.

[20] M.A. Afifi, P.H.R. Pereira, Y.C. Wang, Y.W. Wang, S.K. Li, T.G. Langdon, Effect of ECAP processing on microstructure evolution and dynamic compressive behavior at

different temperatures in an Al-Zn-Mg alloy, Mater. Sci. Eng. A 684 (2017) 617-625.

[21] R. Kapoor, J.B. Singh, J.K. Chakravartty, High strain rate behavior of ultrafine-grained Al-1.5 Mg, Mater. Sci. Eng. A 496 (2008) 308-315.

[22] L. Zhen, G.A. Li, J.S. Zhou, D.Z. Yang, Micro-damage behaviors of Al-6Mg alloy impacted by projectiles with velocities of 1-3.2 km/s, Mater. Sci. Eng. A 391 (2005) 354-366.

[23] W.S. Lee, Z.C. Tang, Relationship between mechanical properties and microstructural response of 6061-T6 aluminum alloy impacted at elevated temperatures, Mater. Des. 58 (2014) 116-124.

[24] M.A. Afifi, Y.C. Wang, T.G. Langdon, Effect of dynamic plastic deformation on the microstructure and mechanical properties of an Al-Zn-Mg alloy, Mater. Sci. Eng. A 784 (2020) 139287.

[25] A.K. Agrawal, A. Singh, Limitations on the hardness increase in 316L stainless steel under dynamic plastic deformation, Mater. Sci. Eng. A 687 (2017) 306-312.

[26] Z.B. Zhang, O.V. Mishin, N.R. Tao, W. Pantleon, Microstructure and annealing behavior of a modified 9Cr-1Mo steel after dynamic plastic deformation to different strains, J. Nucl. Mater, 458 (2015) 64-69.

[27] L.X. Sun, N.R. Tao, M. Kuntz, J.Q. Yu, K. Lu, Annealing-induced hardening in a nanostructured low-carbon steel prepared by using dynamic plastic deformation, J. Mater. Sci. Technol. 30 (2014) 731-735.

[28] Z. Zhang, D. Liu, Y.S. Wang, Y.H. Pang, F.X. Zhang, Y.H. Yang, J.G. Wang, A novel method for preparing bulk ultrafine-grained material: Three dimensional severe plastic deformation. Mater. Lett. 276 (2020) 128209.

[29] F.K. Yan, G.Z. Liu, N.R. Tao, K. Lu, Strength and ductility of 316L austenitic stainless steel strengthened by nano-scale twin bundles, Acta Mater. 60 (2012) 1059-1071.

[30] H.T. Wang, N.R. Tao, K. Lu, Strengthening an austenitic Fe-Mn steel using nanotwinned austenitic grains, Acta Mater. 60 (2012) 4027-4040.

[31] Y.F. Feng, R.B. Song, Z.Z. Pei, R.F. Song, G.Y. Dou, Effect of aging isothermal time on the microstructure and room-temperature impact toughness of Fe-24.8Mn-7.3Al-1.2C austenitic steel with κ-carbides precipitation, Met. Mater. Int. 24 (2018) 1012-1023.

[32] Z.W. Wang, W.J. Lu, H. Zhao, J.Y. He, K. Wang, B.C. Zhou, D. Ponge, D. Raabe, Z.M. Li, Formation mechanism of κ-carbides and deformation behavior in Si-alloyed FeMnAlC lightweight steels, Acta Mater. 198 (2020) 258-270.

[33] F. Brasche, C. Haase, M. Lipinska-Chwalek, J. Mayer, D.A. Molodov, Combined κ-carbide precipitation and recovery enables ultra-high strength and ductility in light-weight steels, Mater. Sci. Eng. A 795 (2020) 139928.

[34] R.V. Penna, L.N. Bartlett, T. Constance, Understanding the role of inclusions on the dynamic fracture toughness of high strength lightweight FeMnAl steels, Int. J. Metalcast. 13 (2019).

[35] J.H. Shin, J.H. Jang, S.D. Kim, S.J. Park, J. Lee, Dynamic strain aging in Fe-Mn-Al-C lightweight steel, Phil. Mag. Lett. 100 (2020) 355-364.

[36] Y.F. Feng, R.B. Song, Y.J. Wang, Z.Z. Pei, The synergistic effect of deformation twins and polycrystalline structure on strain hardening in a high-SFE Fe-Mn-Al-C austenitic cast steel in compression, Mater. Lett. 272 (2020) 127814.

[37] S.Y. Han, S.Y. Shin, S. Lee, N.J. Kim, J. Kwak, K. Chin, Effect of carbon content on cracking phenomenon occurring during cold rolling of three light-weight steel plates, Metall. Mater. Trans. A 42 (2011) 138-146.

[38] C. Zhao, R.B. Song, L.F. Zhang, F.Q. Yang, T. Kang, Effect of annealing temperature on the microstructure and tensile properties of Fe-10Mn-10Al-0.7C low-density steel. Mater. Design 91 (2016) 348-360.

[39] Z. Li, Y.C. Wang, X.W. Cheng, Z.Y. Li, C. Gao, S.K. Li, The effect of rolling and subsequent aging on microstructures and tensile properties of a Fe-Mn-Al-C austenitic steel, Mater. Sci. Eng. A 822 (2021) 141683.

[40] H. Song, J. Yoo, S.S. Sohn, M. Koo, S. Lee, Achievement of high yield strength and strain

hardening rate by forming fine ferrite and dislocation substructures in duplex lightweight steel, Mater. Sci. Eng. A 704 (2017) 287-291.

[41] M.X. Liu, X. Li, Y.H. Zhang, C.J. Song, Q.J. Zhai, Multiphase precipitation and its strengthening mechanism in a V-containing austenite-based low density steel, Intermetallics 134 (2021) 107179.

[42] P. Ren, X.P. Chen, C.Y. Wang, Y.X. Zhou, W.Q. Cao, Q. Liu, Evolution of microstructure, texture and mechanical properties of Fe-30Mn-11Al-1.2C low-density steel during cold rolling, Mater. Charact. 174 (2021) 111013.

[43] Z. Li, Y.C. Wang, X.W. Cheng, Z.Y. Li, J.K. Du, S.K. Li, The effect of Ti-Mo-Nb on the microstructures and tensile properties of a Fe-Mn-Al-C austenitic steel, Mater. Sci. Eng. A 780 (2020) 139220.

[44] T. Ungár, I. Dragomir, Á. Révész, A. Borbély, The contrast factors of dislocations in cubic crystals: the dislocation model of strain anisotropy in practice, J. Appl. Crystallogr. 32 (1999) 992-1002.

[45] T. Ungár, S. Ott, P.G. Sanders, A. Borbély, J.R. Weertman, Dislocations, grain size and planar faults in nanostructured copper determined by high resolution X-ray diffraction and a new procedure of peak profile analysis, Acta Mater. 46 (1998) 3693-3699.

[46] O.A. Zambrano, Stacking fault energy maps of Fe-Mn-Al-C-Si steels: effect of temperature, grain size, and variations in compositions, J. Eng. Mater-T. ASME 138 (2016) 041010

[47] J. A. Castañeda, O.A. Zambrano, G.A. Alcázar, S.A. Rodríguez, J.J. Coronado, Stacking fault energy determination in Fe-Mn-Al-C austenitic steels by X-ray diffraction. Metals-Basel 11(2021) 1701.

[48] Z. Li, Y.C. Wang Y, X.W. Cheng, J.X. Liang, S.K. Li, Compressive behavior of a Fe-Mn-Al-C lightweight steel at different strain rates, Mater. Sci. Eng. A 772 (2020) 138700.

[49] D. Han, H. Ding, D.G. Liu, The microstructures and tensile properties of aged Fe-xMn-8Al-0.8C low-density steels, Mater. Sci. Technol. 36 (2020) 681-689.

[50] K. Choi, C.H. Seo, H. Lee, S.K. Kim, J.H. Kwak, K.G. Chin, K.T. Park, N.J. Kim, Effect of aging on the microstructure and deformation behavior of austenite base lightweight Fe–28Mn–9Al–0.8C steel, Scr. Mater. 63 (2010) 1028-1031.

[51] L. Yang, Z.M. Li, X. Li, Y.H. Zhang, K. Han, C.J. Song, Q.J. Zhai, An enhanced Fe-28Mn-9Al-0.8C lightweight steel by coprecipitation of nanoscale Cu-rich and κ-carbide particles. Steel. Res. Int. 91 (2020) 1900665.

[52] J.D. Yoo, S.W. Hwang, K. Park, Factors influencing the tensile behavior of a Fe-28Mn-9Al-0.8C steel, Mater. Sci. Eng. A 508 (2009) 234–240.

[53] Y. Yang, J.L. Zhang, C.H. Hu, Z.P. Luo, Y.H. Zhang, C.J. Song, Q.J. Zhai, Structures and properties of Fe-(8-16)Mn-9Al-0.8C low density steel made by a centrifugal casting in near-rapid solidification, Mater. Sci. Eng. A 748 (2019) 74-84.

[54] H. Song, Y. Kwon, S.S. Sohn, M. Koo, N.J. Kim, B.J. Lee, Improvement of tensile properties in (austenite+ferrite+κ-carbide) triplex hot-rolled lightweight steels, Mater. Sci. Eng. A 730 (2018) 177-186

[55] H. Ding, H.Y. Li, R.D.K. Misra, Z.Q. Wu, M.H. Cai, Strengthening mechanisms in low density Fe-26Mn-xAl-1C steels. Steel. Res. Int. 89 (2018) 1700381.

[56] A.J. Ardell, Precipitation hardening, Metall. Trans. A (1985) 2131-2165.

[57] Y.Z. Li, Z.C. Luo, Z.Y. Liang, M.X. Huang, Effect of carbon on strain-rate and temperature sensitivity of twinning-induced plasticity steels: modeling and experiments, Acta Mater. 165 (2019) 278-293

Figure Captions：

Fig.1 XRD patterns of the as-received and the DPD processed and post-DPD aged steels

Fig.2 EBSD orientation color map of an as-received sample

Fig.3 EBSD orientation color maps of the steels after DPD processing at strains of (a) 0.25, (b) 0.50, (c) 0.75 and after DPD processing at strains of (d) 0.25, (e) 0.50, (f) 0.75 and post-DPD aging at 450 °C for 2 h

Fig.4 Grain size distributions of the DPD processed samples at strains of (a) 0.25, (c) 0.50, (e) 0.75 and aged samples after DPD at strains of (b) 0.25, (d) 0.50, (f) 0.75

Fig.5 Bright field TEM images of the DPD processed samples at strains of (a) 0.25, (b) 0.50, (c) 0.75 and aged samples after DPD at strains of (d) 0.25, (e) 0.50, (f) 0.75

Fig.6 SEM images of the (a) as-received, (b) DPD-0.25, (c) DPD-0.75 and (d) DPD-0.75-450 samples

Fig.7 Dark field TEM images show the morphologies of κ-carbides in the samples with a strain of 0.75 (a) before and (b) after aging at 450℃

Fig.8 True stress-strain curve of dynamic compression testing of all samples at strain rates of (a) 1.0×10^{-3} s^{-1}, (b) 1.0×10^{0} s^{-1} and (c) 2.0×10^{3} s^{-1}

Fig. 9 Influence of DPD strain on the yield strengths of the DPD processed and post-DPD aged steels at strain rates of (a) 1.0×10^{-3} s^{-1}, (b) 1.0×10^{0} s^{-1}, and (c) 2.0×10^{3} s^{-1}

Fig.10 Contribution of individual strengthening factors to the yield strength at a strain rate of 1.0×10^{-3} s^{-1}

Fig.11 Plots of $ln\dot{\varepsilon}$ as a function of yield stress σ for the steel: the values of K are equal to the slopes of the lines obtained through linear fitting.

Table Legend：

Table 1. Calculated values of strength from different strengthening mechanisms

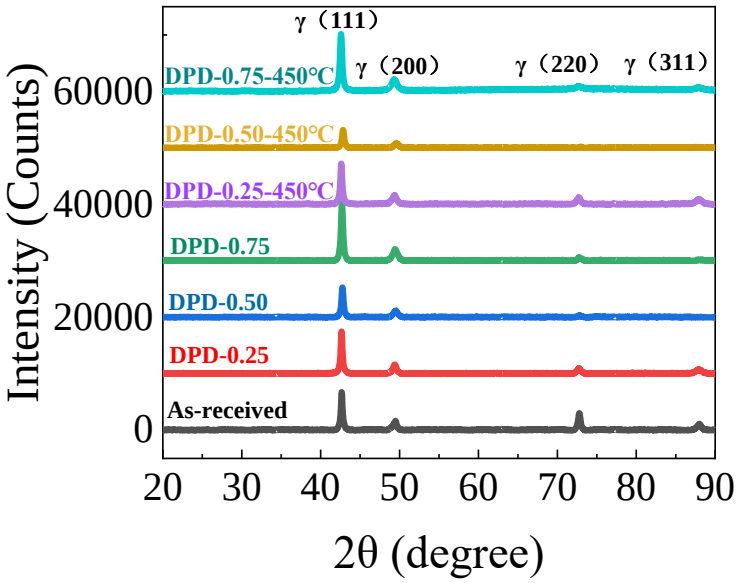

Fig.1 XRD patterns of the as-received and the DPD processed and post-DPD aged steels

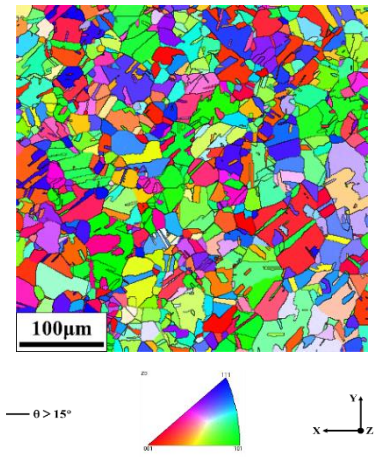

Fig.2 EBSD orientation color map of an as-received sample

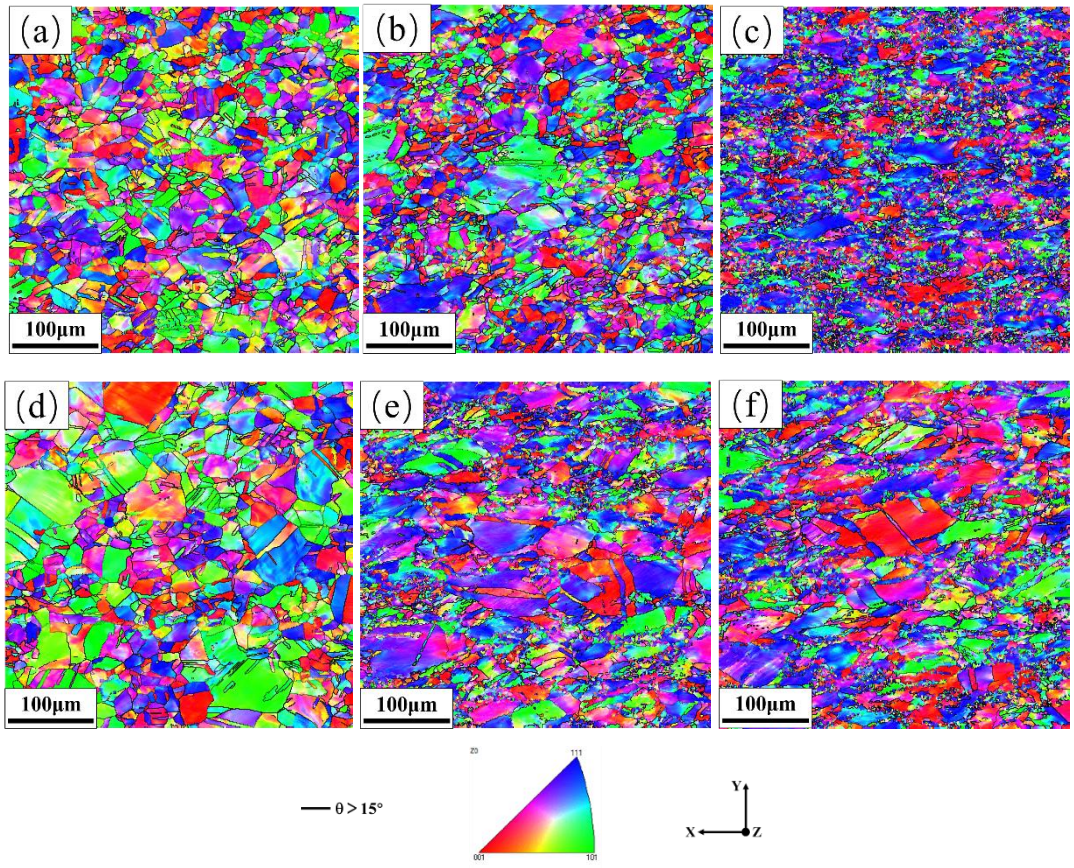

Fig.3 EBSD orientation color maps of the steels after DPD processing at strains of (a) 0.25, (b) 0.50, (c) 0.75 and after DPD processing at strains of (d) 0.25, (e) 0.50, (f) 0.75 and post-DPD aging at 450 °C for 2 h

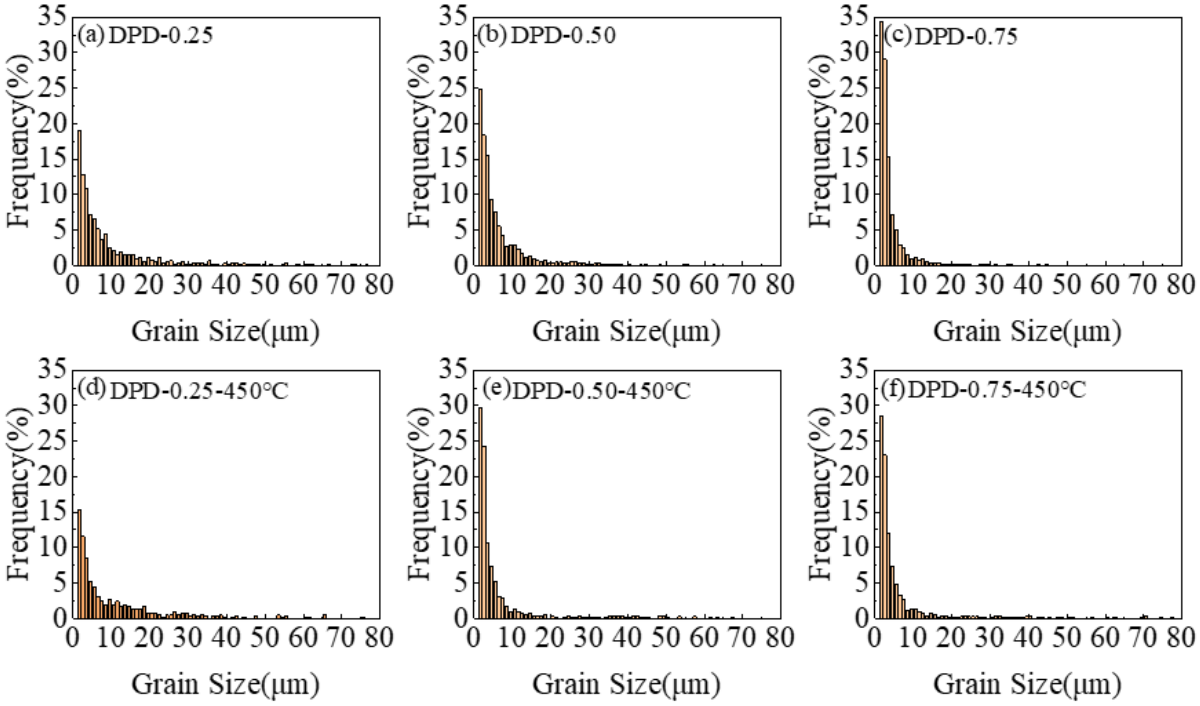

Fig.4 Grain size distribution of the DPD processed samples at strains of (a) 0.25, (c) 0.50, (e) 0.75 and aged samples after DPD at strains of (b) 0.25, (d) 0.50, (f) 0.75

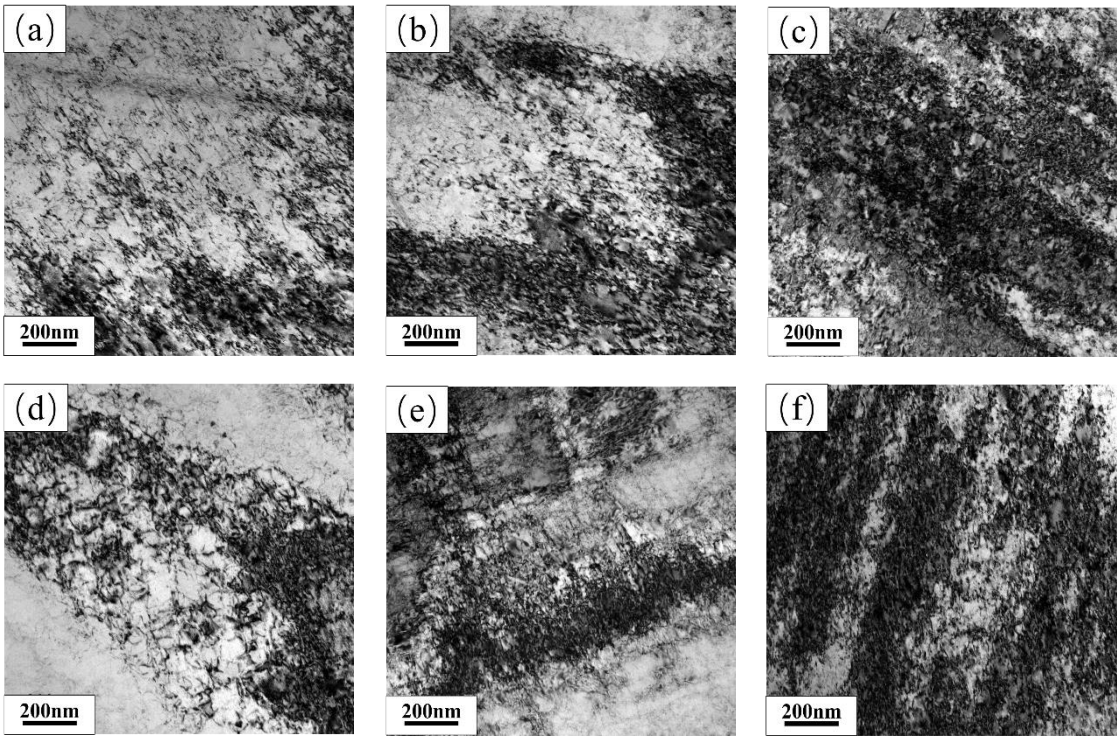

Fig.5 Bright field TEM images of the DPD processed samples at strains of (a) 0.25, (b) 0.50, (c) 0.75 and aged samples after DPD at strains of (d) 0.25, (e) 0.50, (f) 0.75

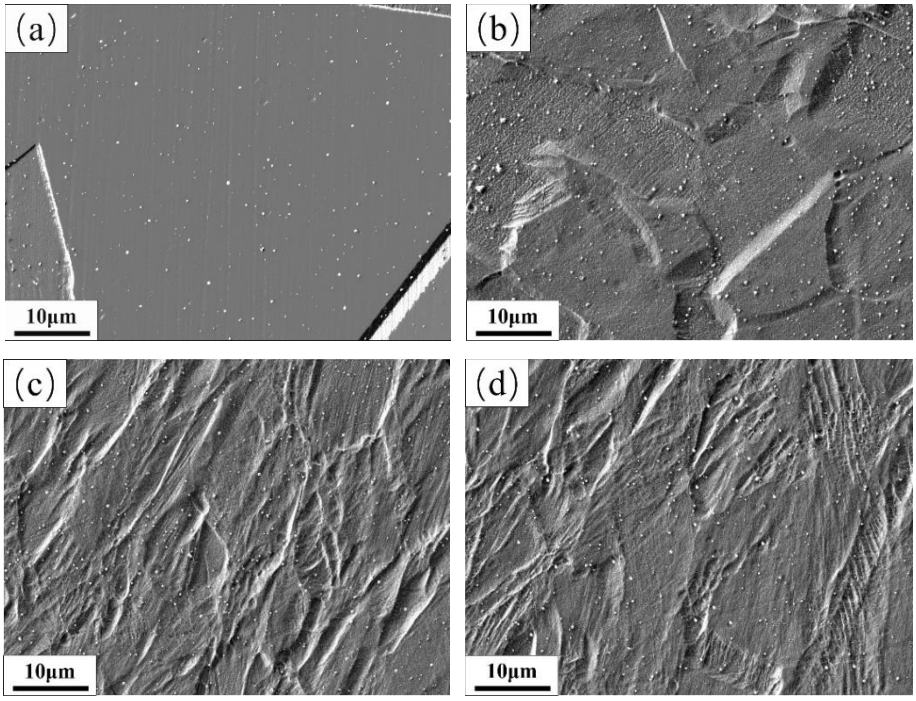

Fig.6 SEM images of the (a) as-received, (b) DPD-0.25, (c) DPD-0.75 and (d) DPD-0.75-450 samples

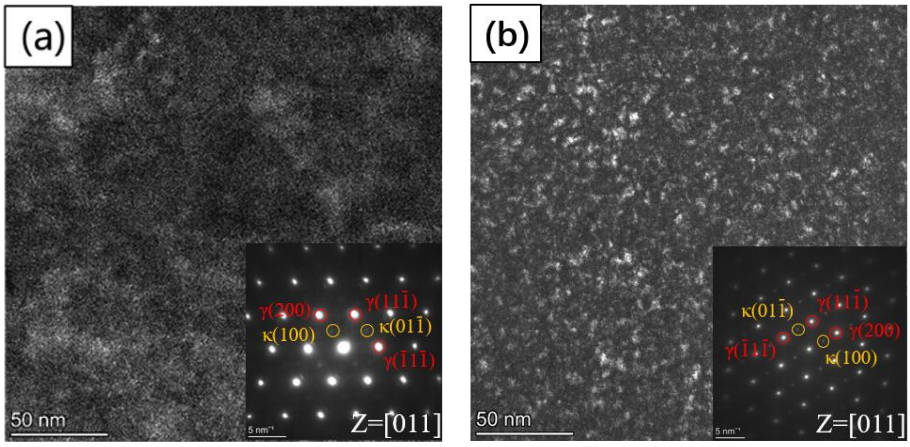

Fig.7 Dark field TEM images show the morphologies of κ-carbides in the samples with a strain of 0.75 (a)before and (b)after aging at 450℃

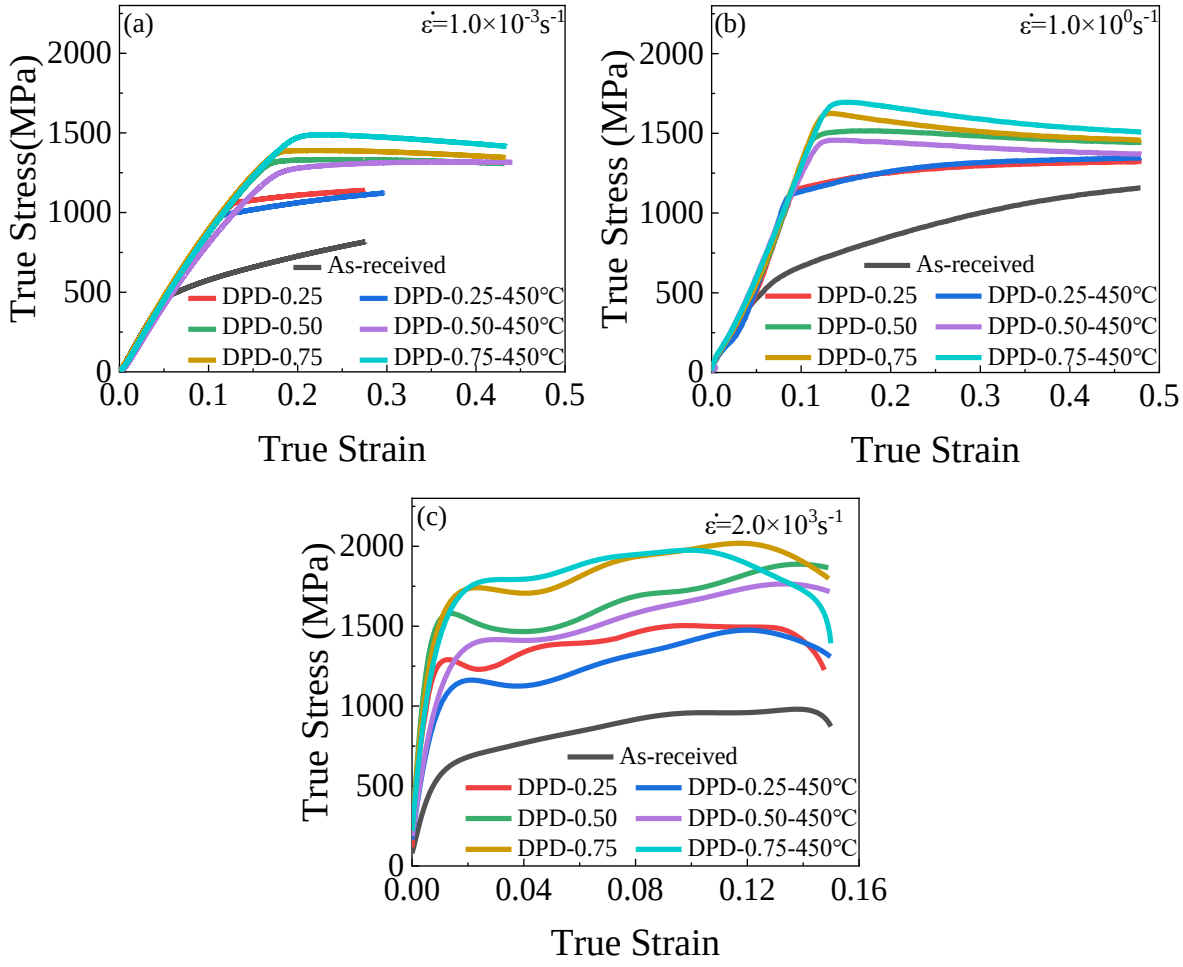

Fig.8 True stress-strain curve of dynamic compression testing of all samples at strain rate of (a) 1.0×10^{-3} s^{-1}, (b) 1.0×10^{0} s^{-1}, and (c) 2.0×10^{3} s^{-1}

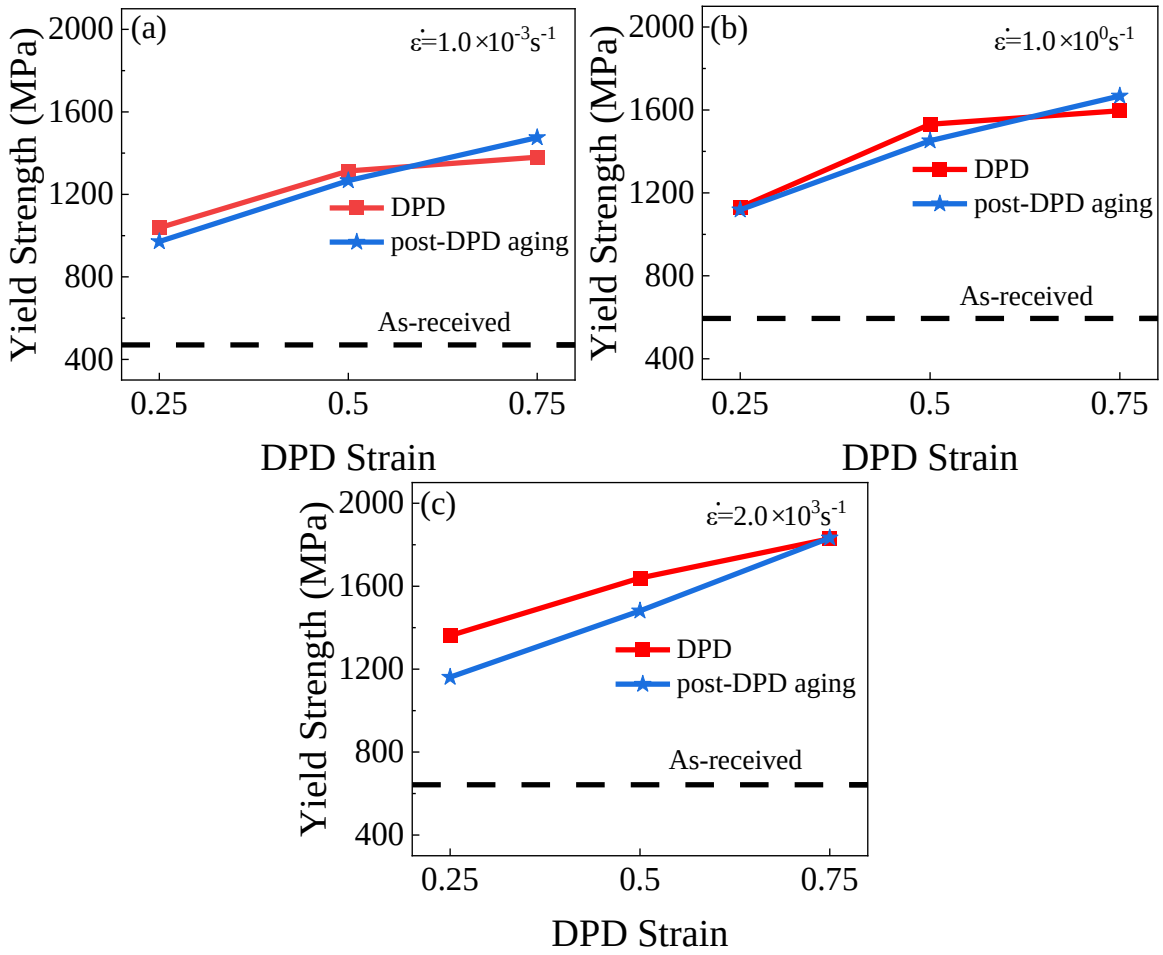

Fig. 9 Influence of DPD strain on the yield strengths of the DPD processed and post-DPD aged steels at strain rates of (a) 1.0×10^{-3} s^{-1}, (b) 1.0×10^{0} s^{-1}, and (c) 2.0×10^{3} s^{-1}

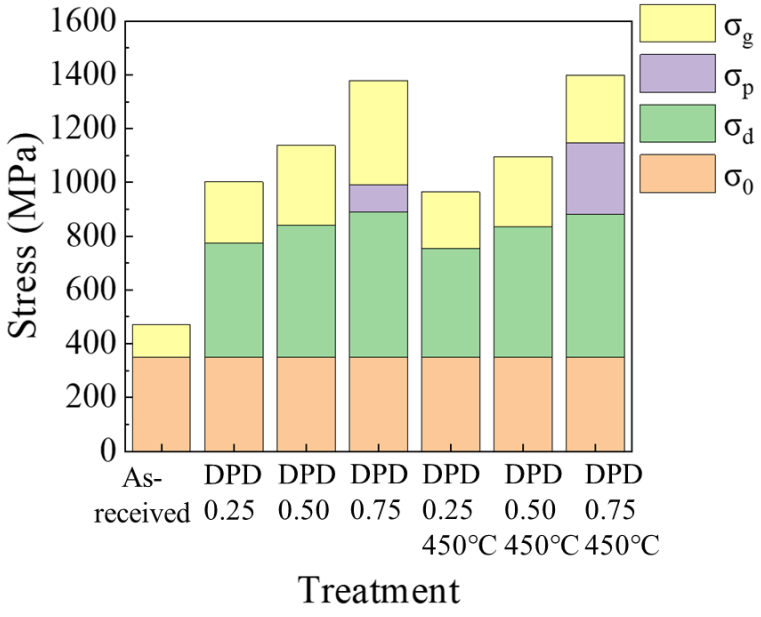

Fig.10 Contribution of individual strengthening factors to the yield strength at a strain rate of 1.0×10^{-3} s^{-1}

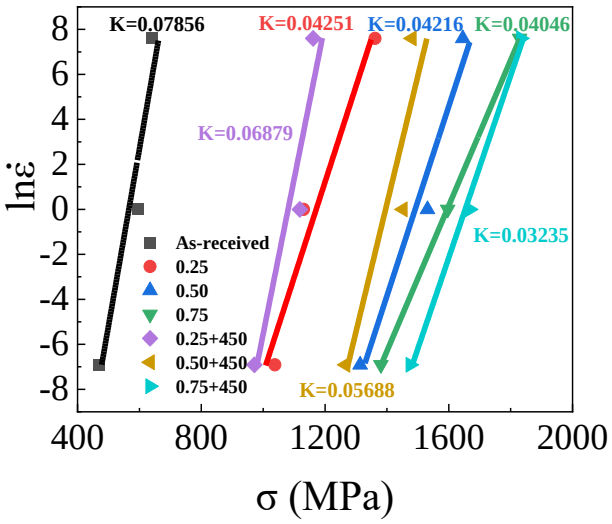

Fig.11 Plots of $ln\dot{\varepsilon}$ as a function of yield stress σ of the steel: the values of K are equal to the slopes of the lines obtained through linear fitting.

Table 1. Calculated values of strength from different strengthening mechanisms

sample	σ_0/MPa	σ_d/MPa	σ_p/MPa	σ_g/MPa
As-received	349	/	/	122
DPD-0.25	349	427	/	226
DPD-0.50	349	493	/	296
DPD-0.75	349	540	101	389
DPD-0.25-450	349	406	/	210
DPD-0.50-450	349	487	/	260
DPD-0.75-450	349	532	266	253